Journal of the American Ceramic Society

High-temperature strength and plastic deformation behavior of niobium diboride consolidated by spark plasma sintering

Journal:	*Journal of the American Ceramic Society*
Manuscript ID	JACERS-39584.R2
Manuscript Type:	Article
Date Submitted by the Author:	22-May-2017
Complete List of Authors:	Demirskyi, Dmytro; Nanyang Technological University, Temasek Laboratories Solodkyi, Ievgen; National Institute for Materials Science (NIMS), Nishimura, Toshiyuki; National Institute for Materials Science, Nano Ceramics Center Sakka, Yoshio; National Institute for Materials Science, Fine Particle Processing Vasylkiv, Oleg; National Institute for Materials Science, Research Center for Functional Materials; Nanyang Technological University, Temasek Laboratories
Keywords:	ultra-high temperature ceramics, strength, spark plasma sintering

High-temperature strength and plastic deformation behavior of niobium diboride consolidated by spark plasma sintering

Dmytro Demirskyi †(a), Ievgen Solodkyi (b), Toshiyuki Nishimura (c), Yoshio Sakka* (b) and Oleg Vasylkiv (b).

(a) Nanyang Technological University, 50 Nanyang Avenue, 639798 Singapore

(b) National Institute for Materials Science, 1-2-1 Sengen, Tsukuba, Ibaraki 305-0047, Japan

(c) National Institute for Materials Science, 1-1 Namiki, Tsukuba, Ibaraki, 305-0044, Japan

Corresponding Author - Dmytro Demirskyi, Nanyang Technological University, 50 Nanyang Avenue, 639798 Singapore, phone: +65-93415641, dmytro.demirskyi@ntu.edu.sg.

Abstract

Bulk niobium diboride ceramics were consolidated by spark plasma sintering (SPS) at 1900 °C. SPS resulted in dense specimens with a density of 98% of the theoretical density and a mean grain size of 6 μm. During the SPS consolidation, the hexagonal boron nitride (h-BN) was formed from B_2O_3 on the powder particle surface and residual adsorbed nitrogen in the raw diboride powder. The room-temperature strength of these NbB_2 bulks was 420 MPa. The flexural strength of the NbB_2 ceramics remained unchanged up to 1600 °C. At 1700 °C an increase in strength to 450 MPa was observed, which was accompanied by the disappearance of the secondary h-BN phase. Finally, at 1800 °C signs of plastic deformation were observed. Fractographic analysis revealed a number of etching pits and steplike surfaces suggestive of high-temperature deformation. The temperature dependence of the flexural strength of NbB_2 bulks prepared by SPS was compared with data for monolithic TiB_2, HfB_2 and ZrB_2. Our analysis suggested that the thermal stresses accumulated during SPS consolidation may lead to additional strengthening at elevated temperatures.

† Author to whom correspondence should be addressed, dmytro.demirskyi@ntu.edu.sg
* Member of American Ceramic Society

Keywords: high-temperature strength; niobium diboride; spark plasma sintering.

1. Introduction

The borides are a highly refractory class of ceramic materials characterized by extreme hardness, high electrical conductivity, and a positive temperature coefficient of electrical resistance. All borides have a metallic appearance, and some are better conductors of electricity than the parent metals. The borides of most interest for high-temperature structural applications are the diborides of chromium, hafnium, niobium, tantalum, titanium, vanadium, and zirconium [1,2].

Niobium diboride (NbB_2) is an AlB_2-type hexagonal compound, which possesses a high melting point (~3050 °C), high hardness (21 GPa), good high-temperature hardness and high electrical conductivity [3–5]. NbB_2 has potential use for structural applications; however, the previous research mainly focused on its superconducting behavior [6,7]. A possible reason for the lack of investigation of monolithic NbB_2 is the relatively low melting temperature of niobium oxides [1,4].

Nevertheless, composites of NbB_2 exhibit some distinctive properties that are currently required for the development of ultra-high-temperature ceramics (UHTCs) [8]. NbB_2–CrB_2 composites exhibit high hardness and oxidation resistance [9]. In addition, B_4C–NbB_2 and SiC–NbB_2 eutectic composites show high fracture toughness (up to 7 $MPa \cdot m^{1/2}$) and hardness (25–30 GPa) in the eutectic and hypereutectic regions [10–12]. SiC–NbB_2 eutectic, in particular, has shown exceptional stability at elevated temperatures with a flexural strength of 600 MPa sustained at 1900 °C.

Owing to the different production methods of NbB_2 ranging from thin films [13] to dense ceramic specimens prepared by hot-pressing [14] or spark plasma sintering (SPS) [3,4] some of its mechanical properties have not been evaluated; to date, the flexural strength of this diboride

has not been reported. This is a significant omission because NbB_2-based ceramics have the potential to be used at high temperatures, and it is important to know their behavior when stressed at high temperatures conditions.

Hence, the present study focuses on the consolidation of bulk NbB_2 ceramic using high-temperature SPS [15–17] at 1900 °C for 10 mins, and the flexural strength of NbB_2 is evaluated using three- and four-point methods. In addition, the high-temperature performance of NbB_2 up to 1800 °C is reported for the first time.

2. Materials and Methods

Commercially available NbB_2 powder (LOT #APG7777, average powder particle size 1.0–2.4 μm, <0.5 wt% C, <0.5 wt% N, <0.7 wt% O (according to the manufacturer specification), Wako Pure Chemical Industries, Ltd., Osaka, Japan) was used in the present study. NbB_2 was homogenized by wet mixing in alcohol, followed by drying at about 100 °C. The resultant powder was screened through 60- and 400-mesh screens.

The homogenized powder was loaded into a graphite die with an inner diameter of 60 mm and subjected to SPS. The outer surface of the die was wrapped in 5-mm-thick graphite felt to homogenize the temperature distribution and reduce heat loss by radiation. The mold system containing the powder mixture was placed in an SPS furnace (HP D125, FCT, Germany). Initially, a pressure of 20 MPa was applied to ensure sufficient electrical contact between the powder tablet and the graphite die, which was then increased to 80 MPa at 800 °C. A dwell time of 1 min at 800 °C was used to increase the pressure. Then we increased the temperature at a rate of 110 °C·min^{-1} up to a sintering temperature of 1900 °C with a dwell time of 10 min. Subsequently, each specimen was gradually cooled to 600 °C at a rate of 100 °C·min^{-1} and then

naturally to room temperature in the furnace. The sintering process was performed in argon gas with a flow rate of 2 $L \cdot min^{-1}$.

The sintered specimens were ground with diamond disks with a particle size of up to 0.5 μm. Then, the density of the samples was measured by the Archimedes method using ethanol as a medium in accordance with ASTM B 963–08.

The three- and four-point flexural strengths were determined using rectangular blocks (2×2.5×26 mm) cut from specimens with a diameter of 60 mm by electric discharge machining. Their lateral surfaces were ground and polished using diamond pastes to a 0.5 μm finish. The flexural strengths were measured by a Shimadzu AG-X plus (Shimadzu, Kyoto, Japan) mechanical strength testing equipment. In the case of three-point bending supports with a span of 16 mm were used. The four-point flexural strength was evaluated using supports with spans of 20/10 mm. Measurements were performed using with a loading speed of 0.5 $mm \cdot min^{-1}$. Eight to fourteen samples were tested at each temperature, and the standard deviation was taken as the measurement accuracy.

Before the flexural strength tests at elevated temperatures, we used the reference bars made from the material with known flexural strength behavior – the commercially-available boron carbide (Bocadur, CeramTec GmbH, Germany). For the high-temperature flexural strength tests, the following heating schedule was used: from room temperature to 200 °C in 10 min and from 200 °C to the testing temperature at a rate of 18 $°C \cdot min^{-1}$. A dwell time of 5 min was employed before the flexural test at the testing temperature. For the tests above 1600 °C, specimens were gradually cooled and heated up to the test temperature with rate of 12 $°C \cdot min^{-1}$. During these heating and cooling procedures the specimen was kept 20 mm bellow the hot-zone used for the

tests. For the tests conducted bellow 1600 °C the specimen was lowered in 5 minutes for exchange without any dwell at the temperature of the test.

After testing at temperature bellow or equal to 1600 °C, cooling from the testing temperature to room temperature was performed at a rate of 20 °C·min^{-1}. We evaluated the elastic modulus (Ef) from the linear portion of the load–displacement curve using the procedure described in ASTM E111–04. Microstructural observations and analyses were carried out on the fractured surfaces using scanning electron microscopy (SEM, SU 8000; Hitachi, Tokyo, Japan). EDX analysis was performed using Miniscope TM-3000 (Hitachi, Tokyo, Japan) in backscattered electrons (BSE). X-ray diffraction (XRD) analysis (Rigaku RINT 2500 HLR, Japan) was performed on fractured specimens after the high-temperature flexural tests, in order to identify the crystalline phases using Cu Kα radiation.

3. Results

The density measurements suggested that the density of consolidated ceramic specimens was over 98% of the theoretical density (TD). The mean grain size of the NbB_2 grains was evaluated to be 6.2±1.3 μm.

Figure 1 shows loading curves for NbB_2 ceramics recorded during the four-point flexural strength tests at different temperatures. No change in the fracture behavior between room temperature and 800 or 1200 °C was observed in the tests; hence, a curve for the room-temperature test is not presented in **Fig. 1**. For the tests performed at 1600 °C, a change in the slope of the curve was observed, indicating a change in the elastic modulus during testing (**Table 1**).

Fractography analysis of the specimen after the flexural strength tests suggested that breakage mainly occurred in an intergranular manner (**Fig. 2**). Some white coin-shaped disks with a diameter of 1–3 μm and a thickness of 100–200 nm were observed for all specimens tested below 1700 °C. EDX and XRD analyses (**Figs. 3** and **4**) suggests that this phase is h-BN. Hexagonal boron nitride (or α-BN) is generally formed in the high-temperature SPS of boron carbide ceramics [17–19] during consolidation in Ar and N_2, and usually enhances the flexural strength of B_4C ceramics. In the case ZrB_2-based composites [20,21] the h-BN was formed by reaction between residual B_2O_3 surface and partial nitrogen pressure in the vacuum or hot press.

In the scope of the present study, the initial NbB_2 powder was found to contain 2.4 to 2.7 wt.% of nitrogen, significantly higher to that provided by the manufacturer (0.5 wt.%). Other possible impurities such as C (0.35wt.%) and O (up to 0.09 wt.%) where within the specification provided by the manufacturer. The total nitrogen, oxygen and carbon contents were analyzed using ON-900 and CS-800 (Eltra GmbH, Haan, Germany).

Hence, the h-BN was formed by reaction between the residual B_2O_3 on the surface of the NbB_2 particles and the nitrogen entrapped in the powder during the SPS consolidation. Furthermore, a trial consolidation of a NbB_2 specimen with diameter of 10 mm at 1800 °C under vacuum using Dr. Sinter Model 1050 (Sumitomo Coal Mining Co. Ltd., Japan) was carried out. Specimen was heated from a temperature of 700 °C using a heating rate of 110 $°C \cdot min^{-1}$ up to a sintering temperature. After 10 min dwell specimen was gradual cooled to 700 °C at a rate of 100 $°C \cdot min^{-1}$. A pressure of 80 MPa was applied at 700 °C and was kept constant during heating, dwell and cooling procedures. The facture surface of the specimen after consolidation revealed the presence of the h-BN grains. This underlines that the h-BN grains form during the SPS processing result from initial powder rather than consolidation conditions.

When h-BN is located in the intergrain areas, it is known to affect the flexural strength [17] since the pull-out of these grains results in additional energy required for fracture. The main difference between the structures fractured at 25–1600 °C was a slight change in the color of the NbB_2 grains due to thermal etching in argon [22]. Furthermore, facets originating from the action of surface diffusion appeared at 1200 °C and were also present at higher temperatures.

After the flexural tests conducted at 1700 °C and 1800 °C, the h-BN secondary phase is no longer present at the fractographs and hence does not play any role in the fracture of NbB_2 ceramics. One may assume that the disappearance of h-BN grains at temperatures of 1700 °C and above is related to the degradation observed for the hot-pressed boron nitride tiles. The latter process is known to be initiated above 1500 °C in an inert atmosphere such as argon or nitrogen [23] and is associated with the formation of boron oxide, which can be easily accelerated above a certain level of oxygen contamination in the inert gas [23,24]. Although it has not been confirmed, it may be presumed that the same holds true for the h-BN grains in the present study. This is because a previous study on non-consolidated h-BN powder suggested that the thermal stability of h-BN nanoplates under air-flow conditions is similar to that of bulk BN tiles [25]. Furthermore, the time required to cool down the specimen from 1700 °C (or 1800 °C) to 1575 °C allows a window of opportunity to complete the degradation of the h-BN flakes on the fractured surfaces that were exposed during the cooling step.

Nevertheless, in the temperature range for the flexural tests under discussion here, 1700 °C to 1800 °C, the contribution of grain pull-outs increases as the fracture becomes intergranular [26]. Some small rectangular stress pits were visible at these temperatures (and also at 1600 °C), which indicate plastic deformation [19].

Finally, at 1800 °C we observed some steps marked by black arrows in **Fig. 2**, which might be due to the plastic deformation observed in **Fig. 1** or to grooving as a consequence of surface diffusion. Although plastic deformation appears to control the fracture at 1800 °C, the specimen has an elastic end to the load–displacement curve starting at a stress of 373 MPa. This has some nonlinear deviations, which in eutectic composites [27] suggests the formation of micro- and macrocracks during fracture, which can be observed during the fracture of layered materials [28]. However, in the present study, this is an indication of fatigue-like creep-induced fracture, which occurred during plastic deformation and was caused by some grains are being separated at specific crystallographic orientation.

4. Discussion

4.1 Analysis of high-temperature strength

Figure 5 summarizes the data on the flexural strength of monolithic diborides of the IV and V transition groups reported to date [22,29,30]. Previous studies on the strength of the diborides of the IV group suggest that a strength not exceeding 250 MPa may be considered as 'normal' (**Fig. 5 (b)**). Therefore, the strength of 420 MPa at 1600 °C can be attributed to a number of factors including (i) a different electronic structure of NbB_2 as a metal diboride of the V group [31], (ii) a specific value of the grain size of the NbB_2 ceramics and (iii) the consolidation method.

In the case of the niobium diboride, the hexagonal AlB_2-type structure is built of hexagonal nets of Nb and triangular nets of pure boron atoms. While a graphitic network of boron atoms is sandwiched by the metal layers in bulk.

Because the crystal structure of NbB_2 is layered, the physical properties are expected to be highly anisotropic. However, mainly because of the inherent difficulty in growing single crystals of

transition metal diborides, in general, due to their high melting points, almost nothing is known how their physical properties vary with crystallographic directions (i.e., internal crystal anisotropy).

Gillies and Lewis [32] conducted line broadening studies of TiB_2, ZrB_2 and NbB_2 and summarized that NbB_2 was highly anisotropic 00*l* reflections (i.e, 002). It was underlined that this behavior is characteristic of that observed in materials having layer structure, where bonding is much weaker between 00*l* planes than in other crystal directions.

In contrast, Otani et al. [33] studied the high-temperature hardness of transition metal diborides and concluded that identical level of hardness between the *a*- and *c*-planes for NbB_2 and TaB_2 single crystals, suggestive a rather small anisotropy. At the same time, ZrB_2 crystals the *c*-plane had 30% higher hardness than the *a*-plane, and thus it was suggested that ZrB_2 grew normal to the *c*-axis.

A study of HfB_2 suggested that the (0001) surface will relax inwards during heating to 2000 °C [34]. This indicates that crystal structures undergo a change at high temperature because of boron desorption.

These findings indirectly suggest that AlB_2-type crystals at elevated temperature experience the intrinsic relaxation. To some extent, this process is governed by the electronic structure of the diboride and the strength of the Me–Me, Me–B and B–B bonds [31,35,36].

The boron–boron bonds are affected by sp^2 combination of the orbits of valence electrons of boron, while the metal–boron bond is a linear combination of *spd* atomic orbits. In general, the B–B bonds may be considered as identical or all diborides, the different degree of brittleness and, more crucially, the different thermal strength of diborides are probably mainly attributable to the different strength of the Me–B bonds [35,36]. The metal–boron bonds depend on the

degree of participation of the incomplete *d* shell in their formation, namely on the capacity of the transition metal's *d* shell to accept part of the valence elections of boron, forming *spd* hybrid bonds. As noted in [35] by Samsonov et al. raising the temperature leads to the destruction of electronic configurations and results in delocalization of the electrons and a reduction in strength. In the analysis of NbC bulks in [36] Samsonov et al. underlined a noticeable localization of the valence electrons at Nb–Nb bond, which reduces the effect due to the delocalization of electrons from sp^3 configuration of carbon atoms.

Studies on the flexural strength of the layered ternary Nb_4AlC_3 and β-Ta_4AlC_3 phases by Hu et al. [37] showed that strength of the Nb-based compound remains constant 311±57 MPa up to 1400 °C. In contrast, Ta-based compound showed a degradation of strength and elastic modulus above 1000 °C. Thus a change in the Me–Me or Me–C bonds for the layered MAX compounds may lead to the better performance at elevated temperatures probably by controlling the temperature of elastic to plastic transformation.

At this point it is impossible to confirm that the process of relaxation of individual crystallographic planes or peculiarities of the localization of the electrons for NbB_2 have a direct influence on its plasticity, and reliable data on bulk poly- and single crystals of different metal diborides may provide additional insight.

Alternatively, the SPS as a consolidation method may be considered as a factor that affects flexural strength. The effect of the gas atmosphere on the mechanical properties of covalent B_4C was analyzed in [17–19]. Recall that the formation of secondary h-BN phase is one of the few phases that can be formed during SPS consolidation, particularly at temperatures higher than 1800 °C. Other phases such as metal carbides, boron carbide, or layered graphite phases can be formed *in situ* during SPS [38–40]. These secondary phases will affect the flexural strength of

specimens subjected to SPS to a certain extent, but also can be used as pinning phases to control the grain size of consolidated ceramics. Furthermore, it is still unclear whether there is any effect of the pulsed electric current on the mechanical properties bulks subjected to SPS. Another factor that may affect the mechanical properties is the thermal gradient, which is one of the features of the SPS process [41,42].

A recent study on ZrB_2–SiC showed that the elevated-temperature strength behavior of these ceramic composites can be manipulated by additional heat treatment of the specimens after hot-pressing at 1950 °C [43]. An increase in strength of 12% compared with that of unannealed ZrB_2–SiC specimens was obtained during testing in air. As noted in [43], this increase may be due to formation of the secondary phases such as BN, as well as Zr-Fe-Co-Si which is formed by the segregation of impurities, or it may be due to a change in dislocation density.

However, the previous study [37] did not suggest that such heat treatment will alter the elevated-temperature strength behavior for ceramics tested in inert atmospheres or whether the temperature of annealing is correlated with the temperature of consolidation or with the temperature of stress accumulation inside ceramic specimens.

4.2 Effect of additional annealing on the elevated-temperature flexural strength

Owing to the abnormal strength behavior of NbB_2 bulks after SPS observed in **Fig. 1**, we attempted to post anneal the specimens mainly to equilibrate the thermal stresses accumulated during the SPS consolidation. This post annealing was conducted at 1300 °C using a high-temperature cell and a 24 GHz microwaves, as described in detail in [44]. Moderate heating and cooling rates of 20 °C·min^{-1} were used during the microwave annealing, which was conducted in argon gas. Forty NbB_2 specimens were annealed, and the strength data for annealed specimens

was averaged using eight specimens for each temperature. After annealing the specimens were cleaned by ultra sound and subjected to polishing to a 0.5 μm finish using diamond abrasives.

We selected the temperature of 1300 °C because earlier reports [45] suggested that stresses inside ZrB_2–SiC composites are formed during cooling starting at 1300–1400 °C. An additional annealing procedure is well known to enhance the mechanical performance of metals, metal alloys, and ceramics prepared by different methods [46–48]. Samsonov and Koval'chenko suggested [42] that an additional annealing procedure allows the structure gradient to be equilibrated and the release of thermal stresses generated by the hot-pressing procedure. Furthermore, Samsonov's analysis in [49] indicated that such annealing can be performed with heating and cooling rates of up to 200 °C·min^{-1} and that a dwell of 15–30 min can be utilized when thermal stress relaxation is the primary target of the procedure. Moreover, annealing performed with heating and cooling rate up to 20°C·min^{-1} can be used when the thermal stress relaxation and the chemical homogenization are required [48,49]. Considering the similarity of the SPS and HP methods, the additional annealing the specimens subjected to SPS may lead to similar results.

One can observe a difference in the load–displacement curves obtained for the NbB_2 bulks annealed by microwave heating at 1300 °C for 30 min in **Fig. 6**. Firstly, the strength of annealed composites was higher at room temperature and at 800 °C, but by no more than 13% (**Table 2**). This was followed by a 10% decrease in strength at 1200 °C and 1600 °C. Taking into account the possible effect of thermal stresses accumulated inside the ceramic after SPS, we propose that the additional annealing resulted in stress release and that during reheating to the testing temperatures of 1200 °C and 1600 °C, stress release does not occur, thus decreasing the strength [12].

The main difference in the strength behavior for the annealed specimens was between the specimens tested at 1700 and 1800 °C. At 1700 °C, the strength was comparable to that measured at 1600 °C, in contrast to the specimen after SPS, where an increase in strength was observed. However, at 1800 °C we observed load–displacement curves that are typical for the plastic fracture of ceramics, indicating that the specimens suffered from creep damage.

Structure analysis of the fractured specimens (**Fig. 7**) suggested similar fracture behavior to that of the specimens after SPS. Surprisingly, some microcracks [50] were observed at room temperature and also at elevated temperatures. Microcracking is frequently observed to occur in two-phase ceramics and is associated with the mismatch between the temperature dependences of the coefficient of thermal expansion (CTE); however, in the case of annealed specimens, such stresses should in theory be minimized. Among the single-phase ceramics, microcracking has been observed in HfB_2, caused by thermal stresses formed during cooling due to the thermal expansion anisotropy of HfB_2 grains, which have a hexagonal crystal structure [51]. For TiB_2, spontaneous microcracking has been observed when the grain size exceeds 15 μm [52], the appearance of microcracks during fracture at 1700 °C in our study is not yet fully understood, as the additional annealing should have reduced the likelihood of microcrack formation. One must also take into account the fact that microwave heating was utilized to anneal the specimens. However, a positive electrical field effect on a fully dense specimen is generally anticipated as a consequence of the inverted temperature gradient profile observed during microwave processing [53]. Hence, it was thought that performing the thermal annealing using a conventional graphite tube furnace and 20 °C·min^{-1} cooling and heating rate might provide additional information on this subject. Such procedure was undertaken at 1300 °C for 30 min. Six specimens were thus

annealed. Then, two of them where tested at 1600 °C and at 1700 °C, and a single specimen and room temperature and at 1800 °C.

Figure 8 illustrates a typical fracture surface of the NbB_2 bar tested by the four-point method at (a) 1600 °C and (b,c) at 1700 °C. The microcracks were present in all inspected specimens, therefore it most likely that the intrinsic microcracking similar to that in [52] is active for NbB_2. In terms of the flexural strength of conventionally annealed specimens, the measured strengths were within those presented in **Table 2** or **Fig. 6**, and did not exceeded 360 MPa at elevated temperatures. Based on these results, it is thought that the duration and temperature of the additional annealing should be optimized in future.

4.3 Fracture analysis of NbB_2 ceramics after bending tests at 1800 °C

A noticeable difference for the structure of the specimens tested at 1800 °C was the presence of fine subgrains in the grain-boundary area or at triple points. EDX measurements suggested that these subgrains have an almost stoichiometric Nb to B atomic ratio for NbB_2, indicating that they are formed during fracture and are not a consequence of an oxidation process, which may occur locally during flexural strength measurements [29].

Other features observed in **Fig. 2** are intergranular fracture and steplike grooves. Kalish et al. [26] reported that intergranular fracture was mainly observed for ZrB_2 and HfB_2 ceramics tested at 1200 and 1400 °C. NbB_2 bulks follow the same trend, because a fracture mechanism with lower energy dominates at higher temperatures. Nevertheless, the previous studies on bulk transition-metal diborides [26,29,30] did not contain fractographic data on ceramics tested at 1800 °C or above. Since these compounds are representatives of a single family and possess an identical AlB_2 crystal structure, it is likely that other diborides will undergo identical fracture to

that presented in **Figs. 2** and **7 (d)**. The steps that can be clearly seen for the specimens tested at 1800 °C should be formed as a consequence of the high-temperature deformation process, grooves should be formed by the surface diffusion or fatigue-like fracture as a consequence of the ongoing creep process. Recent studies on TiB_2-based ceramics [22,39] illustrated that even at 1600 °C the formation of fine surface markings can be observed on the grain faces, while at 1800 °C the plasticity of titanium diboride was mainly associated with the appearance of 'softened' grains with internal cavities or nonspherical pores (i.e., cavitated grains). Such grains were also observed at 1400 and 1600 °C [39], but at 1800 °C their number increased considerably. We suggest that the structures observed in the present study, namely, the subgrains and the steps on the grain faces, and those [22,39] are formed in different stages of a complex creep-induced high-temperature fracture process for transition-metals diborides; further in-depth studies of the fracture process at temperatures of 1800 °C and above may provide data to increase the understanding of this phenomenon.

Another important observation is that the additional annealing did not affect the grain size of the NbB_2 bulks or the distribution or amount of the secondary h-BN phase. Thus, the difference in the temperature dependence may be explained by the release of thermal stresses during the additional annealing. It is still unclear whether such a relatively rapid post-SPS procedure results in full stress release. As can be seen from [43], a change in the annealing temperature can affect the flexural strength, namely, the optimal temperature for post-SPS annealing may be different from 1300 °C used in the present study.

Nevertheless, even the annealed NbB_2 specimens show high flexural strength compared with those of other bulk monolithic diborides of the IV transition-metal group (**Fig. 3**). The values at

1700 and 1800 °C also appear to be abnormally high compared with those of the IV group diborides, and may explain the high strengths observed for the SiC–NbB_2 system [12].

The two-stage loading-displacement curve (plastic–elastic) observed for the unannealed NbB_2 specimens at 1800 °C requires additional consideration as it appeared to be different from the typical plastic behavior observed for annealed specimens.

We discuss three issues associated with the above results. Firstly, it would be logically to assume that such behavior is connected with the measurement error. The NbB_2 specimen might reach a critical level of plastic deformation and then fracture elastically at a local peak in the compressive/tensile stress ratio. This hypothesis was resected owing to the following observations: (i) this fracture behavior was observed in both the three-point and four-point setups, and (ii) the macroscopical difference between the annealed and unannealed specimens after tests at 1800 °C was in the curvature of the deformation. The latter appears to be logical as unannealed specimens showed higher strain values at 1800 °C (compare **Figs. 1** and **6**). Furthermore, according to [54–56], the measured strengths of ceramics at elevated temperatures are dependent on the loading rate. Thus, further investigation under different loading rates might provide additional information.

Secondly, in the case of ZrB_2 ceramics, a strength of 220±18 MPa was observed at 1800 °C [29,30]. The results of [30] were partly affected by the residual oxygen during the flexural strength tests; in the present study we did not observe any niobium oxides by XRD after the flexural strength tests. Some oxide formation was observed at selected fractured grains by EDX; however, this is likely to be absorbed oxygen, as the amount of detected oxygen was usually bellow 8–10 atomic percent (see, for instance, **Fig. 4**), and thus detected niobium oxide phases cannot be attributed to known niobium oxide compounds. It is not yet possible to make a

definitive conclusion on the effect of residual oxygen on the fracture behavior of zirconium diboride, as investigated in [29], as only few fractographs were presented in [30]. Reference [29] did not discuss any microstructures, which could be used to explain the observed strength vs temperature behavior, but the authors claimed that the high-temperature flexural strength would be increased by the use of raw powder with a lower impurity content.

Finally, a general conclusion can be made from [30] that ZrB_2 specimens with a density of over 95% of the TD and a grain size of 6–11 μm had a slightly better performance than those with other grain sizes. Dense ZrB_2 with a grain size of 19.4±13.0 μm was reported in [29]. The data for HfB_2 presented in **Fig. 5 (b)** is for a specimen with a 15 μm grain size and a density of 97% of the TD [30].

Therefore, the abnormal flexural behavior observed in the present study at elevated temperatures can be considered to be a consequence of the specific grain size obtained for NbB_2. Hence, to fully understand the results observed in the present study, the fabrication and high-temperature strength testing of diborides with different grain sizes are suggested as the next step in future research.

4. Conclusions

Dense NbB_2 ceramics with a specimen diameter of 60 mm were prepared by SPS. The NbB_2 bulks had a density of over 98% of the theoretical density and a mean grain size of 6.2±1.3 μm. The flexural strength of this ceramic was measured up to 1800 °C using three- and four-point methods. The strength between room temperature and 1600 °C was 420 MPa and increased to 450 MPa and 480 MPa at 1700 and 1800 °C, respectively. This is abnormal behavior compared with the bulk diborides of Ti, Zr, and Hf. A peculiar load-displacement curve with both plastic

and elastic parts was obtained during the flexural strength test at 1800 °C. This behavior was correlated with the presence of stress pits and cleavage steps, which indicates that plastic fracture occurred during the flexural tests. Additional post-SPS annealing at 1300 °C resulted in a typical plastic load-displacement curve at 1800 °C. The fine subgrains located at the grain boundaries and the grooves on the grains that fractured by an intergranular mechanism suggest that annealed specimens underwent plastic fracture 1800 °C. This indicates that the complex thermal stress conditions during a SPS consolidation may lead to additional strengthening mechanisms that require further exploration.

Acknowledgements

This study was partially financial supported by the Grant-in-Aid for Scientific Research B (No.15H04163) from JSPS. The authors wish to express their appreciation to Dr. H. Kanai (NIMS) for kindly providing access to the SEM equipment.

References

[1] G.V. Samsonov, I.M. Vinitsky, Refractory Compounds. Handbook, Metallurgiya, Moscow, 1976 [in Russian].

[2] W.G. Fahrenholtz, G.E. Hilmas, I.G. Talmy, and J.A. Zaykoski, "Refractory Diborides of Zirconium and Hafnium," *J. Am. Ceram. Soc.*, **90** 1347–1364 (2007).

[3] O. Balci, D. Agaogullari, F Muhaffel, M.L. Ovecoglu, H. Cimenogli, I. Duman, "Effect of sintering techniques on the microstructure and mechanical properties of niobium borides," *J. Eur. Ceram. Soc.*, **36** 3113–3123 (2016).

[4] K. Sairam, J.K. Sonber, T.S.R.Ch. Murthy, C. Subramanian, R.K. Fotedar, R.C. Hubli, "Reaction spark plasma sintering of niobium diboride," *Int. J. Refract. Met. Hard Mater.*, **43** 259–262 (2014).

[5] K. Nakano, K. Nakamura, T. Okubo, "High temperature hardness and slip system of NbB2 and TaB2 single crystals," *J. Less-Common Met.*, **84** 79–85 (1982).

[6] I.R. Shein, A.L. Ivanovskii, "Band structure of ZrB2, VB2, NbB2, and TaB2 hexagonal diborides: Comparison with superconducting MgB2," *Phys. Solid State*, **44** 1833–1839 (2002).

[7] A. Yamamoto, C. Takao, T. Masui, M. Izumi, S. Tajima, "High-pressure synthesis of superconducting Nb1−xB2 (x=0–0.48) with the maximum Tc=9.2 K," *Phys. C.*, **383** 197–206 (2002).

[8] M.M. Opeka, I.G. Talmy, E.J. Wuchina, J.A. Zaykoski, S.J. Causey, "Mechanical, thermal and oxidation properties of refractory hafnium and zirconium compounds," *J. Eur. Ceram. Soc.*, **19** 2405–2414 (1999).

[9] I.G. Talmy, E.J. Wuchina, J.A. Zaykoski, M.M. Opeka, "Properties of ceramics in the NbB2-CrB2 system," *Ceram. Eng. Sci. Proc.*, **3** 128–135 (1996).

[10] D. Demirskyi, Y. Sakka, "In Situ Fabrication of B4C–NbB2 Eutectic Composites by Spark–Plasma Sintering," *J. Am. Ceram. Soc.*, **97** 2376–2379 (2014).

[11] D. Demirskyi, Y. Sakka, "Fabrication, microstructure and properties of in situ synthesized B4C–NbB2 eutectic composites by spark plasma sintering," *J. Ceram. Soc. Jpn.*, **123** 33–37 (2015).

[12] D. Demirskyi, O. Vasylkiv, "Mechanical properties of SiC–NbB2 eutectic composites by in situ spark plasma sintering," *Ceram. Int.*, **42** 19372–19385 (2016).

[13] S. Motojima, K. Sugiyama, Y. Takahashi, "Chemical vapour deposition of niobium diboride (NbB2)," *J. Cryst. Growth*, **30** 233–239 (1975).

[14] Y. Murata, B.R. Miccioli, "Inhibition of grain growth in niobium boride," *Am. Cer. Soc. Bull.*, **50** 182–184 (1971).

[15] D. Demirskyi, Y. Sakka, "High-temperature reaction consolidation of TaC–TiB2 ceramic composites by spark-plasma sintering," *J. Eur. Ceram. Soc.*, **35** 405–410 (2015).

[16] D. Demirskyi, Y. Sakka, O. Vasylkiv, "High-temperature reactive spark plasma consolidation of TiB2-NbC ceramic composites," *Ceram. Int.*, **41** 10828–10834 (2015).

[17] O. Vasylkiv, D. Demirskyi, P. Badica, T. Nishimura, A.I.Y. Tok, Y. Sakka, H. Borodianska, "Room and high temperature flexural failure of spark plasma sintered boron carbide," *Ceram. Int.*, **42** 7001–7013 (2016).

[18] O. Vasylkiv, D. Demirskyi, H. Borodianska, Y. Sakka, P. Badica, "High temperature flexural strength in monolithic boron carbide ceramic obtained from two different raw powders by Spark Plasma Sintering," *J. Ceram. Soc. Jpn*., **124** 587–592 (2016).

[19] P. Badica, H. Borodianska, S. Xie, T. Zhao, D. Demirskyi, P. Li, A.I.Y. Tok, Y. Sakka, O. Vasylkiv, "Toughness control of boron carbide obtained by spark plasma sintering in nitrogen atmosphere," *Ceram. Int.*, **42** 3053–3061 (2014).

[20] C. Sarbu, J. Vleugels, O. Van der Biest, "Phase instability in ZrO2–TiB2 composites," *J. Eur. Ceram. Soc.*, **27** 2203–2220 (2007).

[21] J. Zou, G.-J. Zhang, J. Vleugels, O. Van der Biest, "High temperature strength of hot pressed ZrB2–20 vol% SiC ceramics based on ZrB2 starting powders prepared by different carbo/boro-thermal reduction routes," *J. Eur. Ceram. Soc.*, **33** 1609–1614 (2013).

[22] D. Demirskyi, T. Nishimura, Y. Sakka, O. Vasylkiv, "High-strength TiB2–TaC ceramic composites prepared using reactive spark plasma consolidation," *Ceram. Int.*, **42** 1298–1306 (2016).

[23] J. Eichler, C. Lesniak, "Boron nitride (BN) and BN composites for high-temperature applications," *J. Eur. Ceram. Soc.*, **28** 1105–1109 (2008).

[24] A. Lipp, K. A. Schwetz, K. Hunold, "Hexagonal Boron Nitride: Fabrication, Properties and Applications," *J. Eur. Ceram. Soc.*, **5** 3–9 (1989).

[25] N. Kostoglou, K. Polychronopoulou, C. Rebholz, "Thermal and chemical stability of hexagonal boron nitride (h-BN) nanoplatelets," *Vacuum*, **112** 42–45 (2015)

[26] D. Kalish, E.V. Clougherty, K. Kreder, "Strength, Fracture Mode, and Thermal Stress Resistance of HfB2 and ZrB2," *J. Am. Ceram. Soc.*, **52** 30–36 (1969).

[27] D. Demirskyi, Y. Sakka, O. Vasylkiv, "High-Strength B4C–TaB2 Eutectic Composites Obtained via in situ by Spark Plasma Sintering," *J. Am. Ceram. Soc.*, **99** 2436–2441 (2016).

[28] M. Lugovy, V. Slyunyayev, V. Subbotin, F. Liang, J. Gou, N. Orlovskaya, T. Graule, J. Kuebler, "Mechanical behavior and failure mechanisms of boron carbide based three-layered laminates with weak interfaces," *Ceram. Int.*, **37** 2255–2261 (2011).

[29] E.W. Neuman, G.E. Hilmas, W.G. Fahrenholtz, "Strength of zirconium diboride to 2300°C," *J. Am. Ceram. Soc.*, **96** 47–50 (2013).

[30] W.H. Rhodes, E.V. Clougherty, D. Kalish, Research and development of refractory oxidation-resistant diborides Part II, Volume IV: mechanical properties. OH: Air Force Materials Laboratory, Air Force Systems Command: Wright Patterson Air Force Base, 1970 [Technical report AFML-TR-68-190, Part II, Volume IV].

[31] G.V.Samsonov, I.F. Prydko, L.F.Prydko, Configurational Model of Matter, Naukova Dumka, Kiev, 1971 [in Russian].

[32] D.C. Gillies and D. Lewis, "Bond Strength in Diborides of Some Group IV and V Metals," *J. Less-Common Metals*, 16 [2] 162–163 (1968).

[33] S. Otani, M.M. Korsukova, T. Mitsuhashi, "Floating zone growth and high-temperature hardness of $NbB_2$and TaB_2 single crystals," *J. Cryst. Growth*, **194** 430–433 (1998).

[34] W. Hayami, R. Souda, T. Aizawa, T. Tanaka, "Structural analysis of the HfB2 (0001) surface by impact-collision ion scattering spectroscopy," *Surf. Sci.*, **415** 433–437 (1998).

[35] G.V. Samsonov, V.K. Kharchenko, L.I. Struk, "Static strength of refractory compounds at high temperatures," *Sov. Powder Met. Metal Ceram.*, **7** 206–209 (1968).

[36] G.V. Samsonov, "Strength and plasticity of refractory compounds," *Inorg. Mater. (USSR),* **9** 1680–1687 (1973).

[37] C. Hu, F. Li, L. He, M. Liu, J. Zhang, J. Wang, Y. Bao, J. Wang, Y. Zhou, "*In Situ* Reaction Synthesis, Electrical and Thermal, and Mechanical Properties of Nb4AlC3," *J. Am. Ceram. Soc.*, **91** 2258–2264 (2008).

[38] J. Gonzalez–Julian, K. Jähnert, K. Speer, L. Liu, J. Räthel, M. Knapp, H. Ehrenberg, M. Bram, O. Guillon, "Effect of Internal Current Flow During the Sintering of Zirconium Diboride by Field Assisted Sintering Technology," *J. Am. Ceram. Soc.*, **99** 35–42 (2016).

[39] D. Demirskyi, H. Borodianska, Y. Sakka, O. Vasylkiv, "Ultra-high elevated temperature strength of TiB2-based ceramics consolidated by spark plasma sintering," *J. Eur. Ceram. Soc.*, **37** 393–397 (2017).

[40] D. Demirskyi, O. Vasylkiv, "Consolidation and grain growth of tantalum diboride during spark plasma sintering," *Ceram. Int.*, **42** 16396–16400 (2016).

[41] G. Maizza, S. Grasso, Y. Sakka, T. Noda, O. Ohashi, "Relation between microstructure, properties and spark plasma sintering (SPS) parameters of pure ultrafine WC powder," *Sci. Tech. Adv. Mater.*, **8** 644–654 (2007).

[42] S. Grasso, T. Saunders, H. Porwal, B. Milsom, A. Tudball, M. Reece, "Flash Spark Plasma Sintering (FSPS) of α and β SiC," *J. Am. Ceram. Soc.*, **99** 1534–1543 (2016).

[43] E.W. Neuman, G.E. Hilmas, W.G. Fahrenholtz, "Elevated Temperature Strength Enhancement of ZrB2-30 vol% SiC Ceramics by Postsintering Thermal Annealing," *J. Am. Ceram. Soc.*, **99** 962–970 (2016).

[44] D. Demirskyi, O. Vasylkiv, Microstructure and mechanical properties of boron suboxide ceramics prepared by pressureless microwave sintering, *Ceram. Int.*, **42** 14282–14286 (2016).

[45] J. Watts, G. Hilmas, W.G. Fahrenholtz, D. Brown, B. Clausen, "Measurement of thermal residual stresses in ZrB2–SiC composites," *J. Eur. Ceram. Soc.*, **31** 1811–1820 (2011).

[46] F.A. McClintock and A.S. Argon, Mechanical Behavior of Materials [Russian translation], Metallurgiya, Moscow, 1970, pp. 224–227.

[47] D Sciti, S Guicciardi, A Bellosi, "Effect of annealing treatments on microstructure and mechanical properties of liquid-phase-sintered silicon carbide," *J. Eur. Ceram. Soc.*, **21** 621–632 (2001).

[48] G.V. Samsonov, M.S. Koval'chenko, Hot Pressing, Gostekhizdat Ukr. SSR, Kiev, 1962, pp. 93–94 [in Russian].

[49] G.V. Samsonov, "Some physical and chemical properties of transition metal compounds with boron, carbon, nitrogen and silicon," (Dr. Sci. Thesis), Moscow institute for non-ferrous metals and gold (1956), pp. 179–183 [in Russian].

[50] L.S. Sigl and H.J. Kleebe, "Microcracking in B4C-TiB2 Composites," *J. Am. Ceram. Soc.*, **78** 2374–2380 (1995).

[51] H.J. Brown-Shaklee, W.G. Fahrenholtz, G.E. Hilmas, "Densification Behavior and Microstructure Evolution of Hot-Pressed HfB2," *J. Am. Ceram. Soc.*, **94** 49–58 (2011).

[52] H.R. Baumgartner, R.A. Steiger, "Sintering and properties of titanium diboride made from powder synthesized in a plasma-arc heater," *J. Am. Ceram. Soc.*, **67** 207–212 (1984).

[53] J. Binner, J. Wang, B. Vaidhyanathan, N. Joomun, J. Kilner, G. Dimitrakis, T.E. Cross, "Evidence for the Microwave Effect During the Annealing of Zinc Oxide," *J. Am. Ceram. Soc.*, **90** 2693–2697 (2007).

[54] E.W. Neuman, G.E. Hilmas, W.G. Fahrenholtz, "Mechanical behavior of zirconium diboride–silicon carbide–boron carbide ceramics up to 2200 C," *J. Eur. Ceram. Soc.*, **35** 463–476 (2015).

[55] ASTM C1211-13, Standard test method for flexural strength of advanced ceramics at elevated temperatures. West Conshohocken, PA: ASTM International, 2013.

[56] J.-X. Liu, G.-J. Zhang, F.-F. Xu, W.-W. Wu, H.-T. Liu, Y. Sakka, T. Nishimura, T.S. Suzuki, D.-W. Ni, J. Zou, "Densification, microstructure evolution and mechanical properties of WC doped HfB2–SiC ceramics," *J. Eur. Ceram. Soc.*, **35** 2707–2714 (2015).

Tables

Table 1 Elevated-temperature mechanical properties of the NbB_2 ceramics

Temperature, °C	Crosshead rate, $mm \cdot min^{-1}$	Number of specimens tested (3P/4P)	Flexural strength, MPa		Elastic modulus, Ef, GPa
			3P	4P	
RT	0.5	14/12	414±17	418±14	542±13
800	0.5	8/8	416±14	420±15	538±10
1200	0.5	8/14	413±16	417±12	534±14
1600	0.5	10/9	415±14	422±17	343±23
1700	0.5	12/9	455±9	471±7	334±17
1800	0.5	8/9	472±5	481±32	-

Table 2 Flexural strength of the annealed NbB_2 ceramics at elevated temperatures

Temperature, °C	Crosshead rate, $mm \cdot min^{-1}$	Four-point flexural strength, MPa‡	Change in flexural strength, σsps / σann, a.u.
RT	0.5	465±21	0.89
800	0.5	481±17	0.87
1200	0.5	381±15	1.09
1600	0.5	367±16	1.14
1700	0.5	366±19	1.28
1800	0.5	351±20	1.37

‡ – flexural strength was averaged by measuring eight bars at each temperature

Figure captions

Figure 1. Typical loading diagrams of NbB_2 ceramics tested at different temperatures by four-point flexural testing. The room-temperature strength test data is not shown since it overlaps with the curves obtained at 800 and 1200 °C. Numbers indicate measured stresses at different points of the loading curve for the specimen tested at 1800 °C.

Figure 2. Microstructures of fractured surfaces of NbB_2 ceramics after flexural strength testing at different testing temperatures (× 5000). The black arrows in the sample tested at 1800 °C indicate the location of steps associated with high-temperature surface diffusion and may correspond to the cracking that occurred, as can be seen from the final part of the loading curve presented in **Fig. 1**.

Figure 3. XRD pattern of the NbB_2 specimen after flexural strength test at 1200 °C. Inset shows a dashed area where a peak that corresponds to (002) plane of the h-BN (#34-0421) can be observed. All other peaks were identified as niobium diboride according to the card #35-0742.

Figure 4. EDX analysis of the fractured surface of the NbB_2 specimen after flexural strength tests at 1200 °C. X-ray mapping of the N Kα in red indicates that BN phase in mainly located in the intergrain areas.

Figure 5. The high-temperature flexural strength of transition metal diborides. (a) shows temperature dependence of strength for NbB_2 ceramic consolidated by SPS. (b) provides data on the high-temperature flexural behavior of other diborides in Argon and Air [22,29,30]. The dashed for ZrB_2 ceramics indicate the general tendencies observed in previous studies [29,30]. Closed symbols indicate that the strength was measured using a four-point setup and the open symbols show the results of three-point flexural strength tests.

Figure 6. Typical loading diagrams of the NbB_2 ceramics subjected to post-SPS annealing at 1300 °C tested at elevated temperatures by four-point flexural testing. Data for the room temperature and 1200 °C tests is not shown for clarity.

Figure 7. Microstructures of fractured surfaces of NbB_2 ceramic specimens subjected to post-SPS microwave annealing after flexural strength test at different testing temperatures: (a) room temperature, (b) 1600 °C, (c) 1700 °C, and (d) 1800 °C. Arrows indicate locations where microcracking occurred during fracture. Note that a different magnification was used in (c) to show the microcracks.

Figure 8. Microstructures of fractured surfaces of NbB_2 ceramic specimens after flexural strength test at (a) 1600 °C and (b,c) 1700 °C. These specimens were subjected to the conventional heating during post-SPS annealing procedure. Arrows indicate locations where microcracking occurred during fracture.

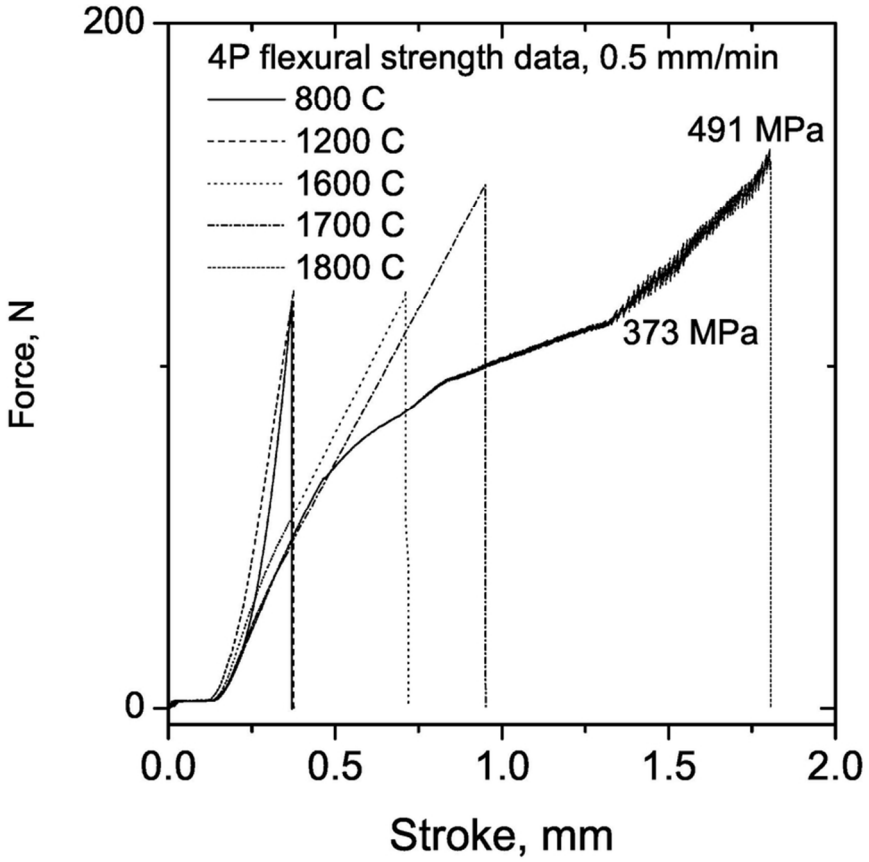

Figure 1. Typical loading diagrams of NbB_2 ceramics tested at different temperatures by four-point flexural testing. The room-temperature strength test data is not shown since it overlaps with the curves obtained at 800 and 1200 °C. Numbers indicate measured stresses at different points of the loading curve for the specimen tested at 1800 °C.

83x84mm (300 x 300 DPI)

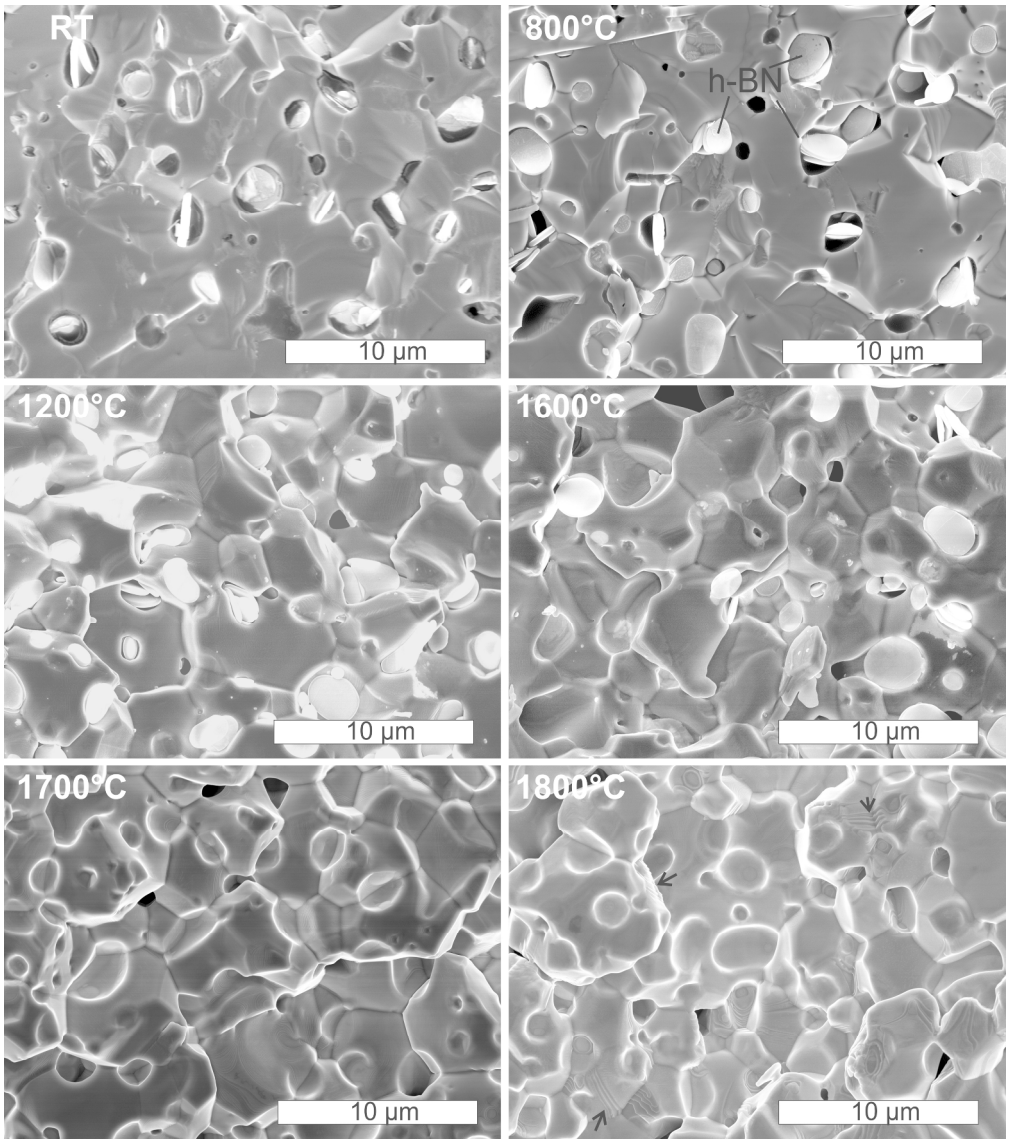

Figure 2. Microstructures of fractured surfaces of NbB_2 ceramics after flexural strength testing at different testing temperatures (× 5000). The black arrows in the sample tested at 1800 °C indicate the location of steps associated with high-temperature surface diffusion and may correspond to the cracking that occurred, as can be seen from the final part of the loading curve presented in **Fig. 1**.

255x289mm (300 x 300 DPI)

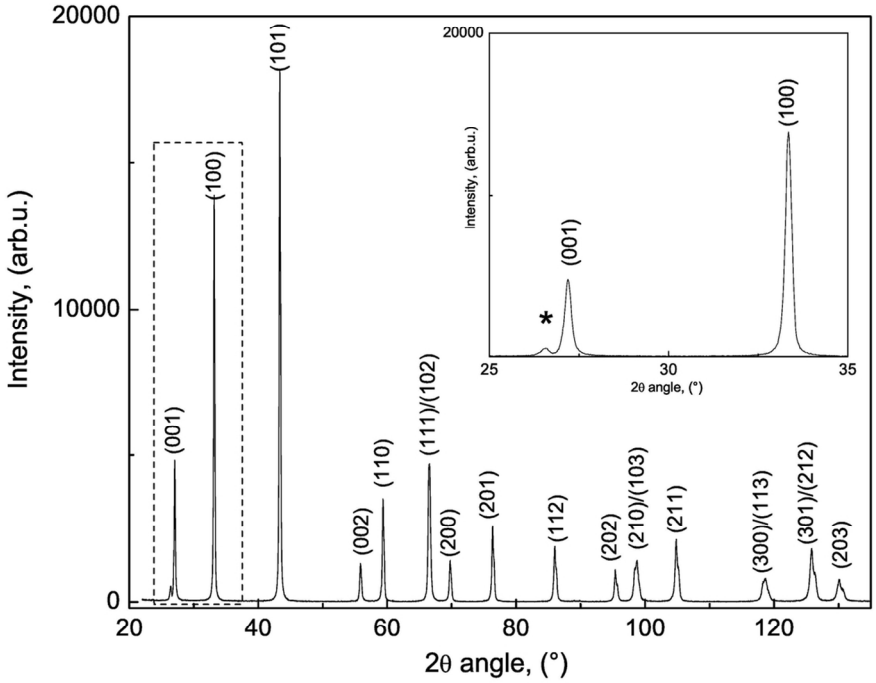

Figure 3. XRD pattern of the NbB_2 specimen after flexural strength test at 1200 °C. Inset shows a dashed area where a peak that corresponds to (002) plane of the h-BN (#34-0421) can be observed. All other peaks were identified as niobium diboride according to the card #35-0742.

109x87mm (300 x 300 DPI)

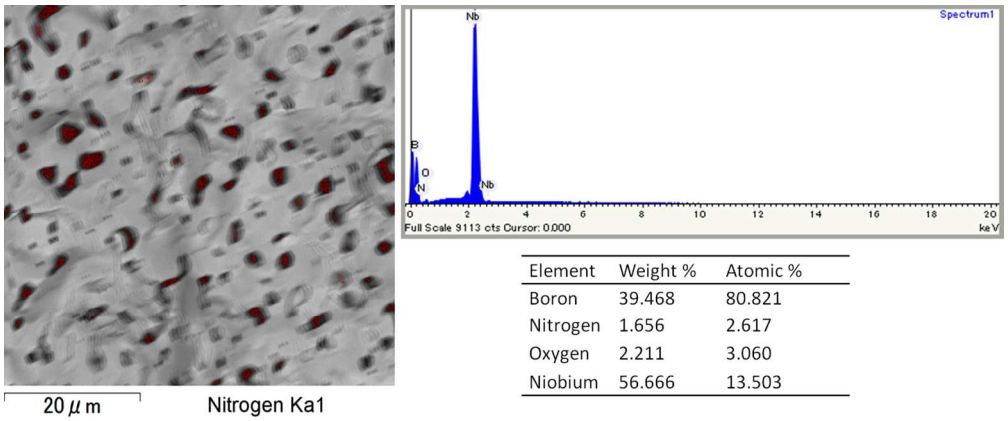

Element	Weight %	Atomic %
Boron	39.468	80.821
Nitrogen	1.656	2.617
Oxygen	2.211	3.060
Niobium	56.666	13.503

Figure 4. EDX analysis of the fractured surface of the NbB_2 specimen after flexural strength tests at 1200 °C. X-ray mapping of the N Kα in red indicates that BN phase in mainly located in the intergrain areas.

245x101mm (150 x 150 DPI)

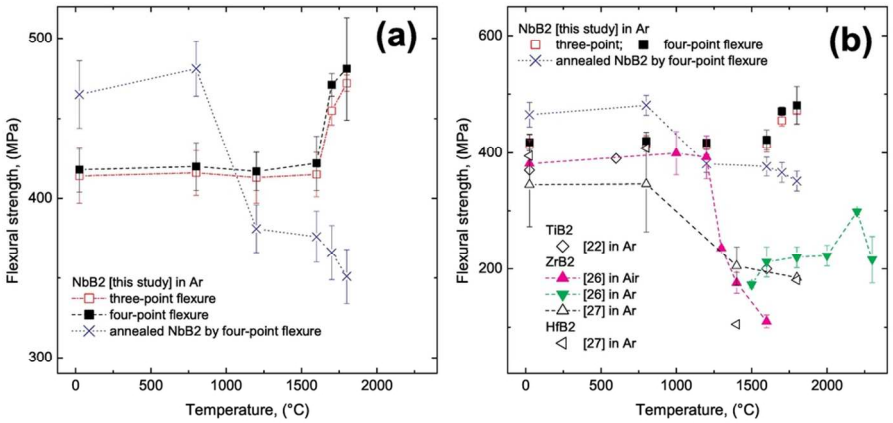

Figure 5. The high-temperature flexural strength of transition metal diborides. (a) shows temperature dependence of strength for NbB_2 ceramic consolidated by SPS. (b) provides data on the high-temperature flexural behavior of other diborides in Argon and Air [22,29,30]. The dashed for ZrB_2 ceramics indicate the general tendencies observed in previous studies [29,30]. Closed symbols indicate that the strength was measured using a four-point setup and the open symbols show the results of three-point flexural strength tests.

99x53mm (300 x 300 DPI)

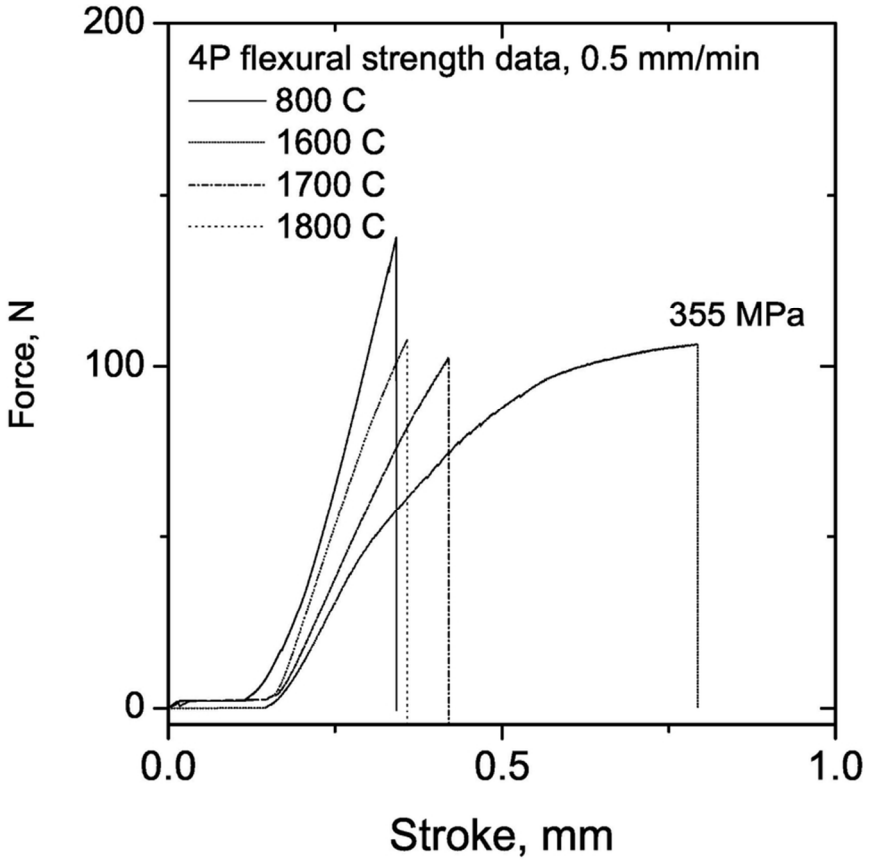

Figure 6. Typical loading diagrams of the NbB_2 ceramics subjected to post-SPS annealing at 1300 °C tested at elevated temperatures by four-point flexural testing. Data for the room temperature and 1200 °C tests is not shown for clarity.

83x84mm (300 x 300 DPI)

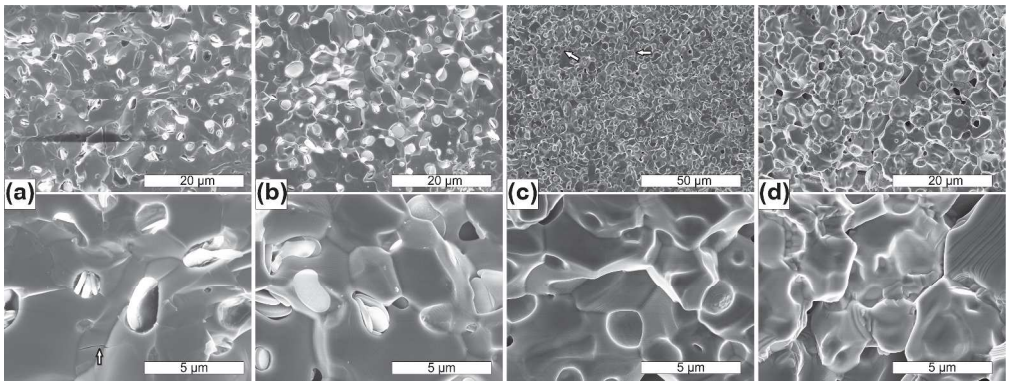

Figure 7. Microstructures of fractured surfaces of NbB_2 ceramic specimens subjected to post-SPS microwave annealing after flexural strength test at different testing temperatures: (a) room temperature, (b) 1600 °C, (c) 1700 °C, and (d) 1800 °C. Arrows indicate locations where microcracking occurred during fracture. Note that a different magnification was used in (c) to show the microcracks.

514x192mm (300 x 300 DPI)

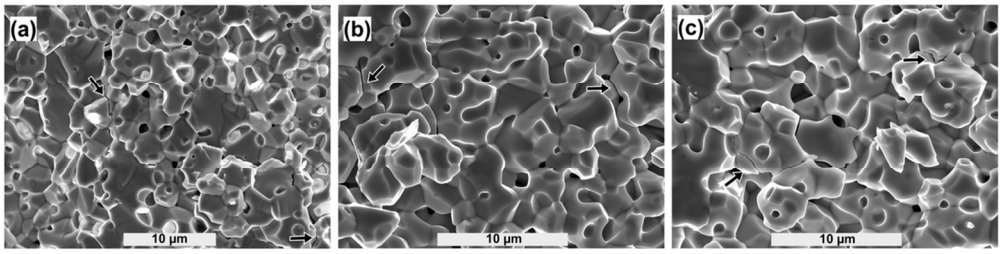

Figure 8. Microstructures of fractured surfaces of NbB_2 ceramic specimens after flexural strength test at (a) 1600 °C and (b,c) 1700 °C. These specimens were subjected to the conventional heating during post-SPS annealing procedure. Arrows indicate locations where microcracking occurred during fracture.

99x25mm (300 x 300 DPI)

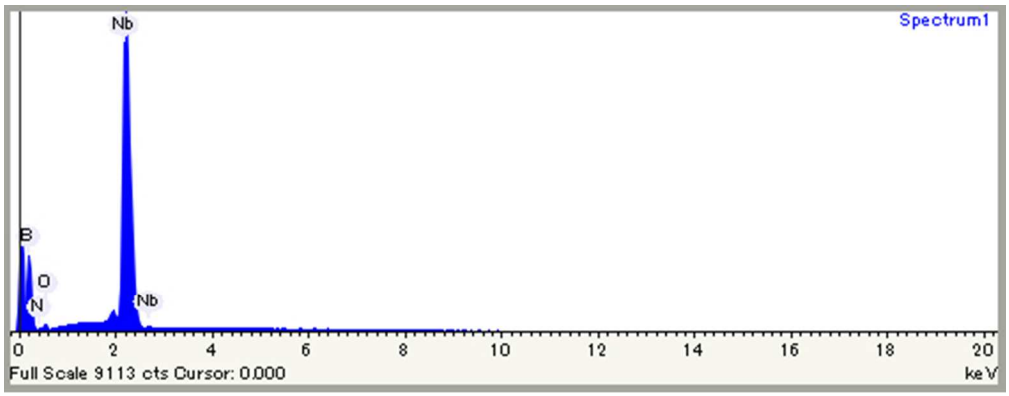

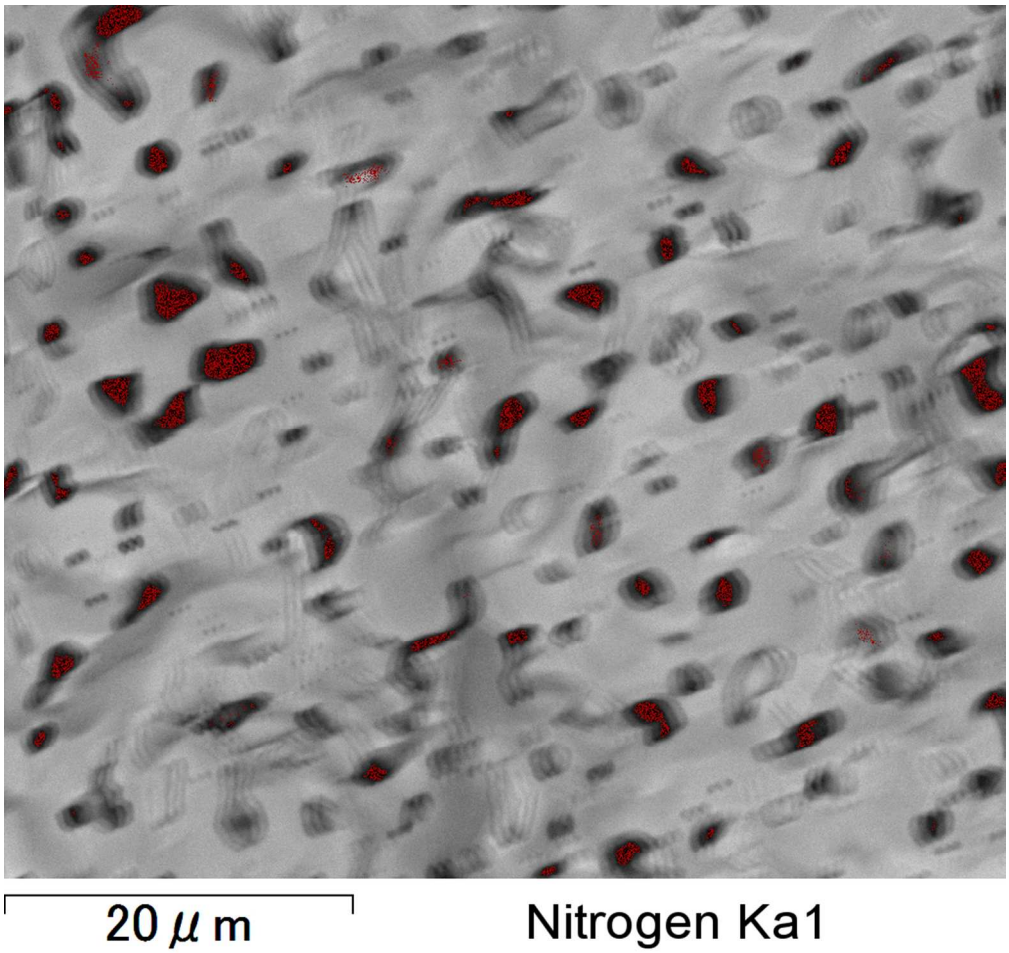

325x344mm (80 x 72 DPI)

Summary results

Element	Weight %	Weight % σ	Atomic %
Boron	39.468	1.212	80.821
Nitrogen	1.656	0.771	2.617
Oxygen	2.211	0.278	3.060
Niobium	56.666	1.193	13.503